Scaling features of a breathing circular billiard

2008 J. Phys. A: Math. Theor. 41 365101

(http://iopscience.iop.org/1751-8121/41/36/365101)

IOP PUBLISHING JOURNAL OF PHYSICS A: MATHEMATICAL AND THEORETICAL

J. Phys. A: Math. Theor. **41** (2008) 365101 (13pp) doi:10.1088/1751-8113/41/36/365101

Scaling features of a breathing circular billiard

Denis Gouvêa Ladeira and Jafferson Kamphorst Leal da Silva

Departamento de Física, ICEx, Universidade Federal de Minas Gerais, Caixa Postal 702, 30.123-970, Belo Horizonte/MG, Brazil

E-mail: dgl@fisica.ufmg.br and jaff@fisica.ufmg.br

Received 8 May 2008, in final form 9 July 2008
Published 6 August 2008
Online at stacks.iop.org/JPhysA/41/365101

Abstract

We investigate the chaotic lowest energy region of the simplified breathing circular billiard, a two-dimensional generalization of the Fermi model. When the oscillation amplitude of the breathing boundary is small and we are near the integrable to non-integrable transition, we obtain numerically that average quantities can be described by scaling functions. We also show that the map that describes this model is locally equivalent to Chirikov's standard map in the region of the phase space near the first invariant spanning curve.

PACS numbers: 05.45.−a, 05.45.Pq

(Some figures in this article are in colour only in the electronic version)

1. Introduction

Since Fermi reported his model to describe the cosmic ray acceleration [1], different models have been developed and studied under different applications. The simplest one-dimensional case, the Fermi–Ulam model [2, 3], consists of a classical particle bouncing between a fixed wall and a moving one. Pustylnikov proposed the bouncer model [4], a variation of the Fermi model in which a particle under gravitational acceleration hits an oscillating platform. While the former model does not present unlimited energy growth, the so-called Fermi acceleration, due to existence of invariant spanning curves [5], the last model does present it. Such unlimited energy growth occurs for some windows of parameter values and initial conditions due to the accelerator modes [4, 6, 7] and outside these windows due to diffusion in the phase space [8].

In two dimensions, the static case is represented by a billiard. Now a particle moves with constant velocity inside a region of the plane and hits elastically the boundary. These models have been used in classical and statistical mechanics [9], and in quantum physics [10]. The natural generalization of the Fermi model is a billiard with a time-dependent boundary [11–16]. Perhaps the most straightforward of such generalizations is the breathing circular billiard [12]. The model consists of a classical particle confined in the region defined by a circle with time-dependent radius. The particle collides elastically with the boundary and due

to the time dependence of the boundary, the particle gains or loses energy at the collision instants. The particle velocity is described in terms of polar coordinates V_r and V_θ. Due to the angular momentum conservation [12] V_θ is a constant. No Fermi acceleration was found for the breathing circle [12]. Depending on how the boundary moves, a time-dependent ellipse presents this phenomenon [17] or not [11]. On the other hand, the unlimited energy growth was observed in the Lorentz-type dispersing billiards [13, 14] and in the annular billiard [15, 16]. A recent overview and discussion of Fermi acceleration in billiards can be found in [18].

In this work we investigate a simplified breathing circular billiard (SBCB), in which we neglect the displacement of the boundary. However, the momentum transference between the wall and the particle occurs normally. In general, this kind of simplification preserves the main properties of the phase space, speeds up the numerical calculations and allows us to obtain analytical results more easily than for the complete version [3, 7, 19].

In the limit situation where the amplitude of oscillation of the radius is zero, the SBCB reduces to the static circular billiard and the value of V_r immediately after each collision is constant. In this case the system is integrable and does not present chaotic behavior. The time dependence, however, introduces a nonlinear interaction between the particle and the boundary. Now the system presents regions of regular motion, elliptical fixed points surrounded by islands of regular motion and spanning curves. One of these curves limits the chaotic sea of lowest energy and it is called the first invariant spanning curve (FISC).

We present some properties of the phase space of SBCB and describe the position of the FISC in terms of (i) the oscillation amplitude of the boundary and (ii) V_θ. By expanding the time between two collisions in a Taylor series for the radial component of velocity, we show that, near the FISC, the mathematical description of SBCB map is locally equivalent to the standard map [20].

Near the transition from the integrable to the non-integrable regime the dynamics of SBCB is critical and the system presents scaling behavior. In limit of small values of the oscillation amplitude, we obtain the scaling description for the average of the squared value of the radial component velocity. Scaling descriptions for some one-dimensional systems, as the Fermi–Ulam model [21–23], time-dependent wells [24] and also potential barriers [25], can be found in the literature. A waveguide model and the bouncer model were also described under scaling analysis [8, 26]. Since the system dimensionality is, in general, very relevant for the determination of scaling exponents, it is natural to investigate a two-dimensional system and compare its exponents with the ones obtained for one-dimensional models. We investigate the situation when the tangential component of the velocity is smaller than a critical value. We also discuss the difficulties in obtaining the scaling description for big values of V_θ. For values of V_θ small enough, we show that the scaling exponents of SBCB are the same as those of the Fermi–Ulam model [21] near the integrable to non-integrable transition.

This paper is organized as follows. In the next section we describe the model and some of its phase-space properties. In section 3 we present some semi-analytical results for the FISC showing that the map of SBCB is locally equivalent to the standard map. In section 4 we present the scaling description of SBCB. Finally, in section 5 we draw a summary of our conclusions.

2. The simplified circular model

The model under analysis consists of a classical particle confined in a region delimited by a circle. The boundary is time-dependent and its position varies around r_0 according to $r(t') = r_0 + \epsilon \cos(\omega t' + \delta_0)$, where ϵ is the amplitude of oscillation, ω is the frequency and δ_0

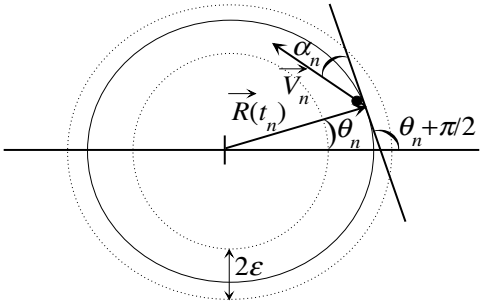

Figure 1. The breathing circular billiard and some of its variables.

the initial phase. It is appropriate to define the dimensionless variables $R(t') = r(t')/r_0$, $t = \omega t'$, $\delta = \omega t' + \delta_0$ and $\varepsilon = \epsilon/r_0$. In figure 1, the breathing circular model as well as some of the dimensionless variables of the system are displayed. The variable θ_n furnishes the angular position of the particle after the nth collision. The variable α_n is the angle between the velocity $\vec{V}_n$ and the line tangent to the circle at θ_n. In terms of θ_n and α_n we have the direction of the vector velocity $\vec{V}_n$. Due to the symmetry of the model, for a given α_0 all possible values of θ_0 are equivalent. Similarly a clockwise ($V_\theta > 0$) or an anticlockwise motion of the particle ($V_\theta < 0$), for the same $|V_\theta|$, does not affect the properties of the system.

We study a simplified version of the model in which we neglect the displacement of the boundary. Due to the momentum angular conservation, the tangential component of the velocity does not change in the collision. Thus we have that $V_{\theta,n+1} = V_{\theta,n} = V_\theta$, with V_θ being a constant of motion. For the SBCB the radial component of the velocity of the particle immediately after a collision is always negative. In terms of dimensionless variables we describe SBCB by the map

$$\vec{V}_{n+1} = -\left|-V_r^{(n)} - 2\varepsilon \sin\delta_{n+1}\right|\hat{r} + V_\theta\hat{\theta}, \qquad \delta_{n+1} = \delta_n + \Delta\delta_{n+1} \bmod 2\pi, \tag{1}$$

where $V_r^{(n)} = -V_n \sin(\alpha_n + \theta_n - \theta_{n+1})$ is the radial component of the velocity immediately before the $(n+1)$th collision. V_n is the modulus of $\vec{V}_n$ (the velocity after the nth collision), and $\hat{r}$ and $\hat{\theta}$ are the radial and angular unitary vectors. Furthermore the quantity $\Delta\delta_{n+1}$ represents the time between two collisions, namely

$$\Delta\delta_{n+1} = \frac{R_{n+1}}{V_n}. \tag{2}$$

Here R_{n+1} is the distance traveled by the particle between the nth and the $(n+1)$th collisions. It can be expressed as follows:

$$R_{n+1} = \sqrt{2[1 - \cos(\theta_{n+1} - \theta_n)]}. \tag{3}$$

The variable α_n and the components of $\vec{V}_n$ are related by

$$\tan\alpha_n = -V_{r,n}/V_\theta. \tag{4}$$

To obtain the value of θ_{n+1} we solve the transcendental equation $f(\theta_{n+1}) = 0$, where $f(\theta_{n+1})$ is given by

$$f(\theta_{n+1}) = \sin\theta_{n+1} - \sin\theta_n + \cot(\alpha_n + \theta_n)(\cos\theta_{n+1} - \cos\theta_n). \tag{5}$$

For $\varepsilon = 0$ the quantities $\theta_{n+1} - \theta_n$ and the radial component of velocity immediately after each collision are constants and the system is integrable. For $\varepsilon \neq 0$, however, the system is nonlinear and the phase space presents regions of chaotic motion. The main focus in this work

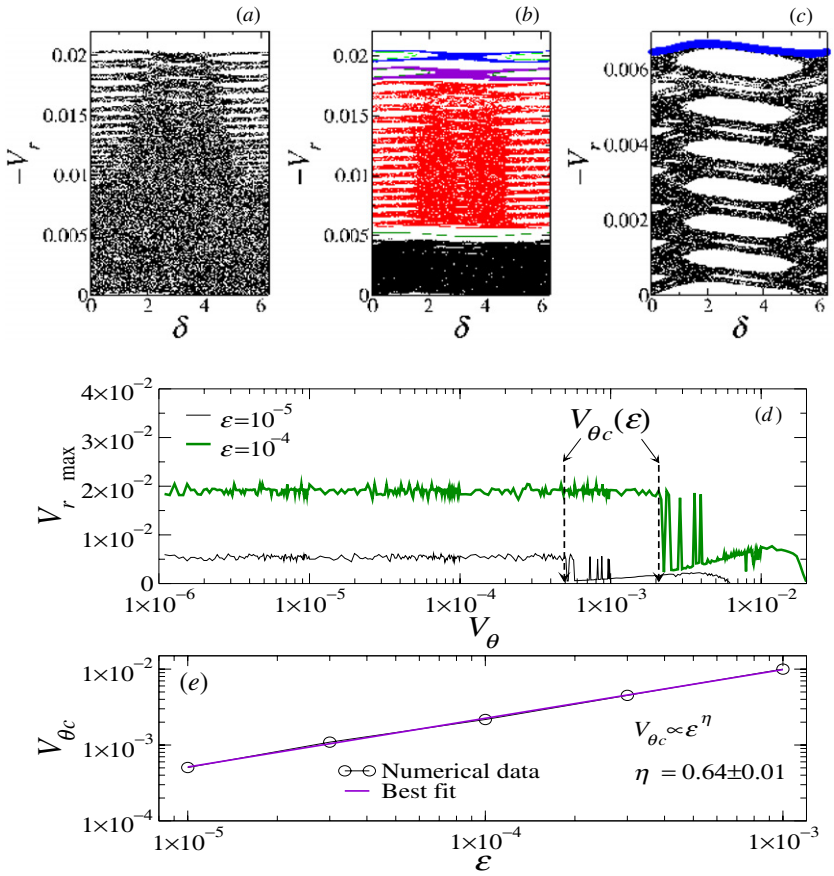

Figure 2. Phase space of SBCB for $\varepsilon = 10^{-4}$ and (*a*) $V_\theta = 10^{-3}$, (*b*) $V_\theta = 5 \times 10^{-3}$ and (*c*) $V_\theta = 1.7 \times 10^{-2}$. (*d*) Maximum absolute value of the radial component of velocity as a function of ε, when the particles are in the lowest chaotic region. (*e*) Dependence of $V_{\theta c}$ on ε.

is on deriving the scaling properties describing this integrable to non-integrable transition. Such an analysis is important because it allows us to compare the scaling descriptions of both one- and two-dimensional versions of the Fermi–Ulam model.

For V_θ small enough the phase space of SBCB is similar to the one-dimensional version. Figure 2(*a*) shows the phase space of the SBCB for $V_\theta = 10^{-3}$ and $\varepsilon = 10^{-4}$. In limit of small values of V_r the phase space presents a mixed structure with a chaotic sea surrounding islands of regular motion. A lowest energy spanning curve, the FISC, limits this chaotic sea. For values of V_r above this spanning curve there are also other observed chaotic regions and islands. We focus the analysis on the lowest energy chaotic region.

The value of V_θ affects the phase space. For $\varepsilon = 10^{-4}$ and $V_\theta = 5 \times 10^{-3}$ we observe that the originally broad chaotic sea of figure 2(*a*) splits into minor chaotic regions, as displayed in figure 2(*b*). This result is a consequence of birth of invariant spanning curves separating the chaotic regions. Thus the position of the first invariant curve depends on the value of V_θ. Figure 2(*c*) shows the structure of the lowest chaotic sea and the FISC for $\varepsilon = 10^{-4}$ and $V_\theta = 1.7 \times 10^{-2}$. Each initial condition in figures 2(*a*)–(*c*) was iterated 10^7 times.

In order to obtain an estimate of the size of the lowest chaotic region for different values of V_θ we iterated the map, equation (1), 10^6 times for an initial condition in the chaotic sea with an initial radial component of the velocity $V_{r0} = 10^{-6}$. Performing this analysis for a fixed value of ε and different values of V_θ we obtained the maximum absolute value of the radial component of the velocity $V_{r\max}$ for the lowest chaotic region. Figure 2(*d*) illustrates the procedure for two values of ε. For small values of V_θ we observe that the value of $V_{r\max}$ is essentially constant. For each value of ε there is a value $V_{\theta c}$ so that for $V_\theta < V_{\theta c}$ the quantity $V_{r\max}$ basically does not depend on V_θ. For $V_\theta \gtrsim V_{\theta c}$ the chaotic regions are so close that numerical errors eventually link them giving the irregular behavior of $V_{r\max}$ that we observe in figure 2(*d*). Finally, for values of V_θ large enough $V_{r\max}$ presents a slow increasing followed by a decreasing (figure 2(*d*)). For very large values of V_θ, not displayed in the figure, the value of V_θ becomes much larger than $V_{r\max}$. Furthermore the quantity $\theta_{n+1} - \theta_n \approx 0$ and, according to equation (3), $R_{n+1} \approx 0$ as well. Therefore in limit of very large values of V_θ the map does not work efficiently because a large number of collisions must occur to provide a small displacement in variable θ. By varying V_θ we obtain $V_{\theta c}$ for different values of ε. Figure 2(*e*) displays the result of this analysis. We have that $V_{\theta c} \propto \varepsilon^\eta$, where $\eta = 0.64 \pm 0.01$.

3. Local equivalency between the SBCB map and the standard map

In this section we present a semi-analytical approximation for the localization of FISC position in the phase space of the SBCB. Similar procedures were employed in [7, 19] for the one-dimensional version of the Fermi–Ulam model. However for the SBCB we must take into account the dependence of the FISC on both parameters ε and V_θ.

We define V_r^* as the characteristic value of the radial component of the velocity near the FISC. Then we expand $\Delta\delta_{n+1}$, equation (2), in Taylor series for $V_{r,n} \approx V_r^*$. Thus we have, until first order,

$$\Delta\delta_{n+1} \approx \left.\frac{R_{n+1}}{V_n}\right|_{V_{r,n}=V_r^*} + \left.\frac{\partial\Delta\delta_{n+1}}{\partial V_{r,n}}\right|_{V_{r,n}=V_r^*} (V_{r,n} - V_r^*), \tag{6}$$

where

$$\frac{\partial\Delta\delta_{n+1}}{\partial V_{r,n}} = V_n^{-1}\frac{\partial R_{n+1}}{\partial V_{r,n}} + R_{n+1}\frac{\partial V_n^{-1}}{\partial V_{r,n}}. \tag{7}$$

Note that the models can only be *locally* equivalents. Therefore we assume that the quantity $(V_{r,n} - V_r^*)$ is small enough and we neglect the terms of order higher than the first in the Taylor expansion. From equation (3) we obtain the first derivative of the right-hand side of the above equation

$$\frac{\partial R_{n+1}}{\partial V_{r,n}} = \frac{\sin(\theta_{n+1} - \theta_n)}{R_{n+1}}\frac{\partial\theta_{n+1}}{\partial V_{r,n}}. \tag{8}$$

In order to obtain $\partial\theta_{n+1}/\partial V_{r,n}$ we employ equation (5) and evaluate $\partial f/\partial V_{r,n} = 0$. This procedure furnishes

$$\frac{\partial\theta_{n+1}}{\partial V_{r,n}} = -[\sin\alpha_n \csc(\alpha_n + \theta_n - \theta_{n+1}) - 1]\frac{\partial\alpha_n}{\partial V_{r,n}}. \tag{9}$$

It follows from equation (4) that

$$\frac{\partial\alpha_n}{\partial V_{r,n}} = -\frac{V_\theta}{V_n^2}, \tag{10}$$

where $V_n^2 = V_\theta^2 + V_{r,n}^2$. Thus, defining

$$\Theta_{n+1} = \frac{\sin(\theta_{n+1} - \theta_n)}{R_{n+1}}[\sin\alpha_n \csc(\alpha_n + \theta_n - \theta_{n+1}) - 1] \tag{11}$$

equation (8) becomes

$$\frac{\partial R_{n+1}}{\partial V_{r,n}} = \Theta_{n+1}\frac{V_\theta}{V_n^2}. \tag{12}$$

We obtain the second derivative of equation (7) in a more straightforward way,

$$\frac{\partial V_n^{-1}}{\partial V_{r,n}} = -\frac{V_{r,n}}{V_n^3}. \tag{13}$$

Substituting equations (12) and (13) into equations (7) and (6) we have

$$\Delta\delta_{n+1}(V_{r,n} \approx V_r^*) = \frac{R_{n+1}^*}{V^*} + \frac{\Delta V_{r,n}}{V^{*3}}(\Theta_{n+1}^* V_\theta - R_{n+1}^* V_r^*), \tag{14}$$

where $V^* = \sqrt{V_r^{*2} + V_\theta^2}$, $\Delta V_{r,n} = V_{r,n} - V_r^*$, and $R_{n+1}^* = R_{n+1}$ evaluated at $V_{r,n} = V_r^*$.

Evaluating equations (3) and (11) numerically we observe that R_n and Θ_n are essentially constant over the first invariant curve. Therefore we define $R^* = R_n^*$ and $\Theta^* = \Theta_n^*$ in the first invariant for all values of n.

Due to the symmetry of SBCB, the radial component of the velocity of the particle immediately after the nth collision, $V_{r,n}$, and immediately before the $(n+1)$th collision, $V_r^{(n)}$, are related by $V_r^{(n)} = -V_{r,n}$. Since V_θ is constant and $V_{r,n} \gg \varepsilon$ in the FISC, we can write that

$$V_{r,n+1} = V_{r,n} - 2\varepsilon \sin\delta_{n+1}. \tag{15}$$

Combining the above equation with $V_{r,n} = V_r^* + \Delta V_{r,n}$ we find the following expression:

$$\Delta V_{r,n+1} = \Delta V_{r,n} - 2\varepsilon \sin\delta_{n+1}.$$

Multiplying both sides of the above equation by $(\Theta^* V_\theta - R^* V_r^*)/V^{*3}$ and adding R^*/V^* to both sides we have

$$\frac{R^*}{V^*} + \frac{\Delta V_{r,n+1}}{V^{*3}}(\Theta^* V_\theta - R^* V_r^*) = \frac{R^*}{V^*} + \frac{\Delta V_{r,n}}{V^{*3}}(\Theta^* V_\theta - R^* V_r^*) - \frac{2\varepsilon}{V^{*3}}(\Theta^* V_\theta - R^* V_r^*)\sin\delta_{n+1}. \tag{16}$$

Comparing equations (14) and (16) we define $I_n = \Delta\delta_{n+1}$ to find

$$I_{n+1} = I_n - K_c \sin\delta_{n+1}, \tag{17}$$

where

$$K_c = K_r + K_\theta, \qquad K_r = -\frac{2\varepsilon}{V^{*3}}R^* V_r^* \qquad \text{and} \qquad K_\theta = \frac{2\varepsilon}{V^{*3}}\Theta^* V_\theta. \tag{18}$$

We evaluated numerically R^* and Θ^* as well as K_r and K_θ for both $V_\theta < V_{\theta c}$ and $V_\theta > V_{\theta c}$, as shown in figures 3(*a*) and (*b*), respectively. In figure 3(*a*) we employed $V_\theta = 10^{-4}$ ($< V_{\theta c}$). We observe that $R^* \approx 2$ for $\varepsilon \in [10^{-5}, 10^{-3}]$ while $|\Theta^*| \ll R^*$. This implies that $|K_\theta| \ll K_r$. Moreover K_c is essentially constant with the average value $K_c = 0.934 \pm 0.008$. In figure 3(*b*) we used $\varepsilon = 10^{-5}$ and different values of V_θ for $V_\theta > V_{\theta c}$. We observe that when V_θ grows, R^* goes to zero and Θ^* increases in absolute value. It follows that K_r approaches zero while K_θ grows. However, the quantity $K_c = K_r + K_\theta$ is basically constant. The average value in this limit is $K_c = -0.92 \pm 0.02$.

For $V_\theta < V_{\theta c}$ we have that $K_c > 0$ and for $V_\theta > V_{\theta c}$ we have that $K_c < 0$. Therefore, near the FISC we define a new variable ϕ and describe the SBCB as

$$I_{n+1} = I_n \pm K_c \sin\phi_n, \qquad \phi_{n+1} = \phi_n + I_{n+1}, \tag{19}$$

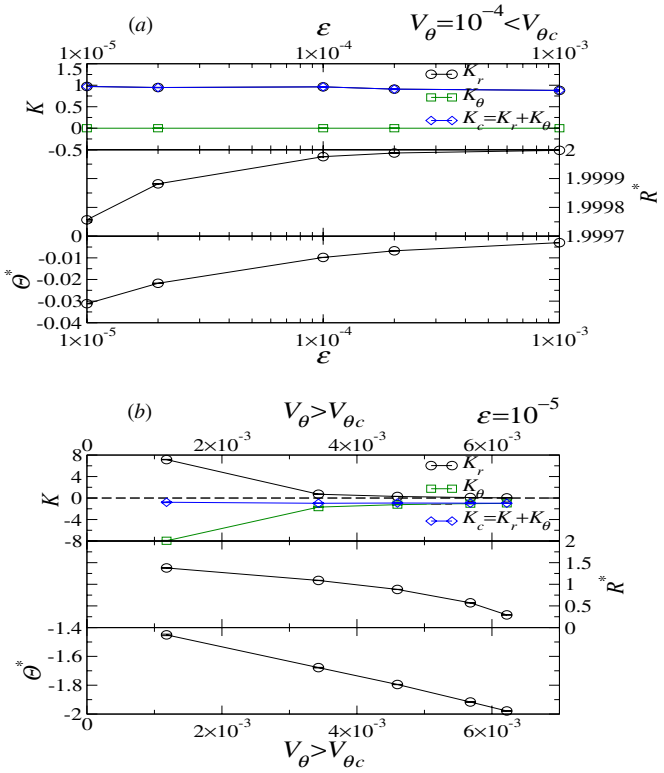

Figure 3. Plot of the values of K, R^* and Θ^* as functions of (*a*) ε for $V_\theta < V_{\theta c}$ ($V_\theta = 10^{-4}$) and (*b*) V_θ ($V_\theta > V_{\theta c}$) for $\varepsilon = 10^{-5}$.

where the plus and minus signals in I expression correspond, respectively, to the situations $V_\theta < V_{\theta c}$ and $V_\theta > V_{\theta c}$. Moreover,

$$\phi_n = \begin{cases} \delta_{n+1} - \pi, & \text{for} \quad V_\theta < V_{\theta c} \\ \delta_{n+1}, & \text{for} \quad V_\theta > V_{\theta c}. \end{cases} \tag{20}$$

Therefore the map that describes the SBCB is locally equivalent to Chirikov's standard map [20]. The signal of K_c changes abruptly at $V_{\theta c}$ and a relation between the variables ϕ and δ is less direct for $V_\theta = V_{\theta c}$. Figures 2(*a*) and (*c*) display the phase space of SBCB for the regimes $V_\theta < V_{\theta c}$ and $V_\theta > V_{\theta c}$, respectively. We stress that we cannot employ arbitrary large values for V_θ because of the numerical limitation of the map.

4. Scaling description

Before starting the scaling analysis, let us define the quantities of interest. We define the average of the squared velocity along an orbit as

$$\overline{V_{r,j}^2}(n) = \frac{1}{n+1} \sum_{i=0}^{n} V_{r,ji}^2.$$

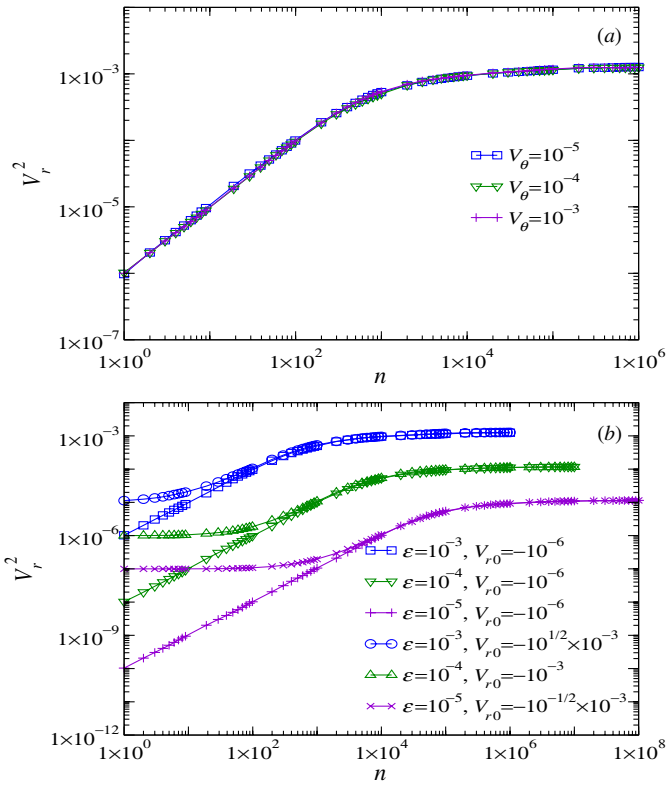

Figure 4. V_r^2 curves as function of n (a) for $\varepsilon = 10^{-3}$ and different values of V_θ, and (b) for different values of ε and V_{r0} with $V_\theta = 10^{-4}$.

Considering an ensemble with M different initial values of δ_0, we evaluate the average quantity as follows:

$$V_r^2(n) = \frac{1}{M}\sum_{j=1}^{M}\overline{V_{r,j}^2}(n). \tag{21}$$

We also used random values for θ_0 but due to the symmetry of the model it does not represent an important detail. Similarly, we always employed positive values of V_θ because the results are affected only by different values of $|V_\theta|$.

We already know from the previous section that the position of the first invariant spanning curve does not depend on V_θ for $V_\theta < V_{\theta c}$. For $\varepsilon = 10^{-3}$ we observe in figure 2(d) that $V_{\theta c} \approx 10^{-2}$. Thus, evaluating the average quantity defined in equation (21), we present in figure 4(a) some curves of V_r^2 as function of n for $\varepsilon = 10^{-3}$ and different values of $V_\theta < 10^{-2}$. We observe that all V_r^2 curves in figure 4(a) are essentially the same because the values of V_θ are smaller than $V_{\theta c}$. Therefore we use $V_\theta = 10^{-4}$ in the next simulations to guarantee that $V_\theta < V_{\theta c}$ for all values of ε employed in the scaling description.

Figure 4(b) shows the behavior of the average quantity V_r^2 defined in equation (21) for different values of ε and V_{r0} as shown in the legend. When the values of V_{r0} are small enough, we observe that the V_r^2 curves grow for small values of n and reach saturation regimes for large n. We define n_x as the value of n that characterizes the changeover from growth to the saturation regime.

For $V_{r0} > \varepsilon$ (see figure 4(*b*)), the V_r^2 curves are essentially constant for small values of n. Subsequently, the V_r^2 curves grow and approach the V_r^2 curves originated from small V_{r0}. The switching from the initial constant value regime of V_r^2 to the growth regime characterizes the crossover value n'_x. Similarly, we define n''_x as the value of n characterizing the changeover from the growth to the saturation regimes. We also observe in figure 4(*b*) that $n_x \approx n''_x$. Moreover the asymptotic regime does not depend on V_{r0}.

For $V_{r0} < \varepsilon$ and small values of n the average V_r^2 depends on both n and ε. Thus, for $n \ll n_x$ we write

$$V_r^2(n, \varepsilon) \propto n^{\alpha} \varepsilon^{\gamma}, \tag{22}$$

where α is the growth exponent and γ establishes the dependence of V_r^2 on ε for small values of n. Performing fittings in the growth regime for eight values of ε in range $[10^{-5}, 2 \times 10^{-3}]$, we obtained the average value $\alpha = 0.995 \pm 0.008$. The best fit in the V_r^2/n^{α} versus ε plot, displayed in figure 5(*a*), furnishes $\gamma = 2.01 \pm 0.01$.

We observe in figure 4(*b*) that the saturation value $V_{r\mathrm{sat}}^2$ depends only on ε. Therefore we write

$$V_{r\mathrm{sat}}^2 \propto \varepsilon^{\beta}, \tag{23}$$

where β is the saturation exponent. We obtained the saturation value $V_{r\mathrm{sat}}^2$ by extrapolation of the V_r^2 curves in limit of large n. Figure 5(*b*) displays the best fit in a $V_{r\mathrm{sat}}^2$ versus ε plot. This procedure furnishes $\beta = 1.013 \pm 0.004$.

The crossover iteration number n_x depends on ε as

$$n_x \propto \varepsilon^{-z}, \tag{24}$$

where z is the dynamical exponent. The intersection between the growth regime and the saturation value $V_{r\mathrm{sat}}^2$ furnishes the crossover value n_x for each value of ε. Figure 5(*c*) shows the ε-dependence of the crossover value n_x. The best fit to the numerical data gives $z = 0.958 \pm 0.008$.

With equations (22)–(24) and the values obtained above for the exponents α, γ, β and z we are ready to start the scaling description. Assuming that the average quantity V_r^2 is a generalized homogeneous function of variables n, ε and V_{r0}, we can write that

$$V_r^2(n, \varepsilon, V_{r0}) = l V_r^2(l^a n, l^b \varepsilon, l^c V_{r0}), \tag{25}$$

where l is an arbitrary scaling factor and a, b and c are scaling exponents. Choosing $l = n^{-1/a}$ the above equation becomes

$$\begin{aligned} V_r^2(n, \varepsilon, V_{r0}) &= n^{-1/a} V_r^2(1, n^{-b/a}\varepsilon, n^{-c/a} V_{r0}) \\ &\propto n^{-(1+xb)/a} \varepsilon^x f(n^{-c/a} V_{r0}). \end{aligned} \tag{26}$$

When $V_{r0} < \varepsilon$, we should have that $f(n^{-c/a} V_{r0})$ is a constant for $n \ll n_x$ (see figure 1(*b*)). Comparing equations (22) and (26) we find $x = \gamma$ and $-(1 + xb)/a = \alpha$.

Choosing $l = \varepsilon^{-1/b}$ equation (25) becomes

$$\begin{aligned} V_r^2(n, \varepsilon, V_{r0}) &= \varepsilon^{-1/b} V_r^2(\varepsilon^{-a/b} n, 1, \varepsilon^{-c/b} V_{r0}) \\ &\propto \varepsilon^{-1/b} g(\varepsilon^{-a/b} n, \varepsilon^{-c/b} V_{r0}). \end{aligned} \tag{27}$$

In limit of large n the V_r^2 curves do not depend either on V_{r0} or on n (figure 1(*b*)). In this case g is a constant. Therefore, comparing equations (23) and (27) we find $-1/b = \beta$.

For $V_{r0} < \varepsilon$ the V_r^2 curves do not depend on V_{r0}. In this way, we have from equation (27) that the crossover value n_x is given by

$$n_x \approx \varepsilon^{a/b}. \tag{28}$$

Comparing equations (24) and (28) we find $z = -a/b$.

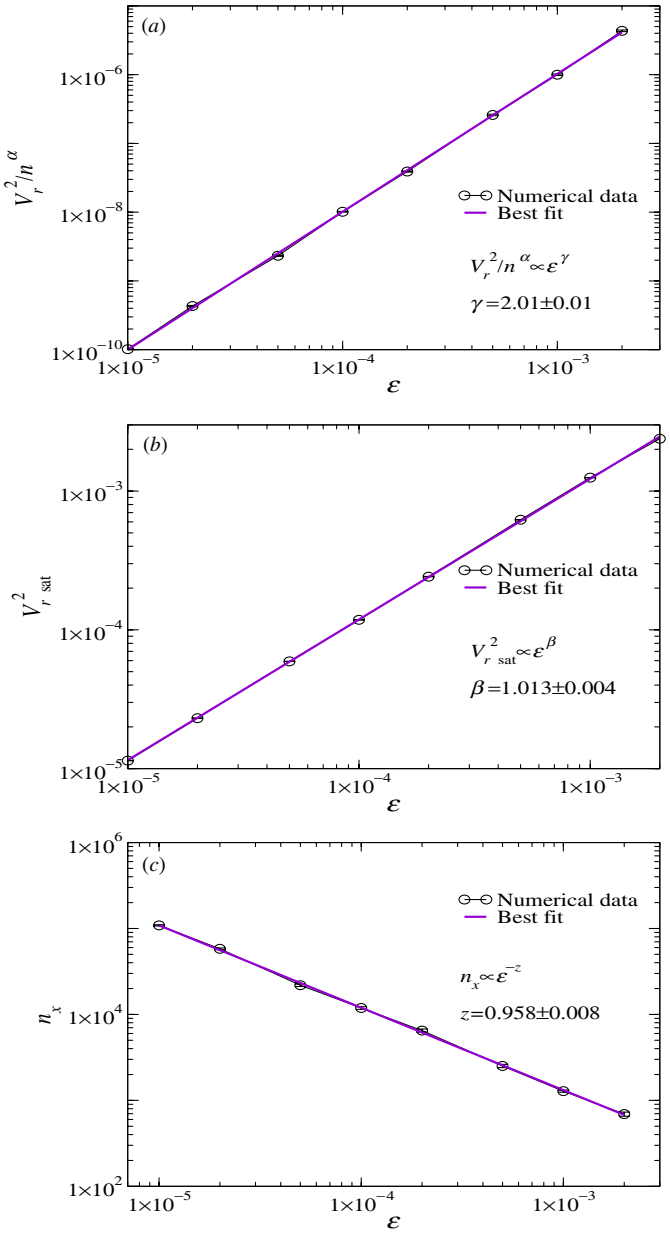

Figure 5. (*a*) Plot of V_r^2/n^α as a function of ε for $n \ll n_x$, (*b*) the ε-dependence of the saturation value $V_{r\mathrm{sat}}^2$ and (*c*) the crossover value n_x versus ε. The best fits to the numerical data furnish, respectively, $\gamma = 2.01 \pm 0.01$, $\beta = 1.013 \pm 0.004$ and $z = 0.958 \pm 0.008$.

For $V_\theta < V_{\theta c}$ we have that $R^* \approx 2$ and that K_r is basically a constant, figure 3(*a*). Moreover K_θ is negligible and $V_r^* \gg V_\theta$. By employing equation (18), we can write that

$$\frac{4\varepsilon}{V_r^{*2}} = \frac{4\varepsilon'}{V_r'^{*2}} = \frac{4l^b\varepsilon}{l^{2c}V_r^{*2}},$$

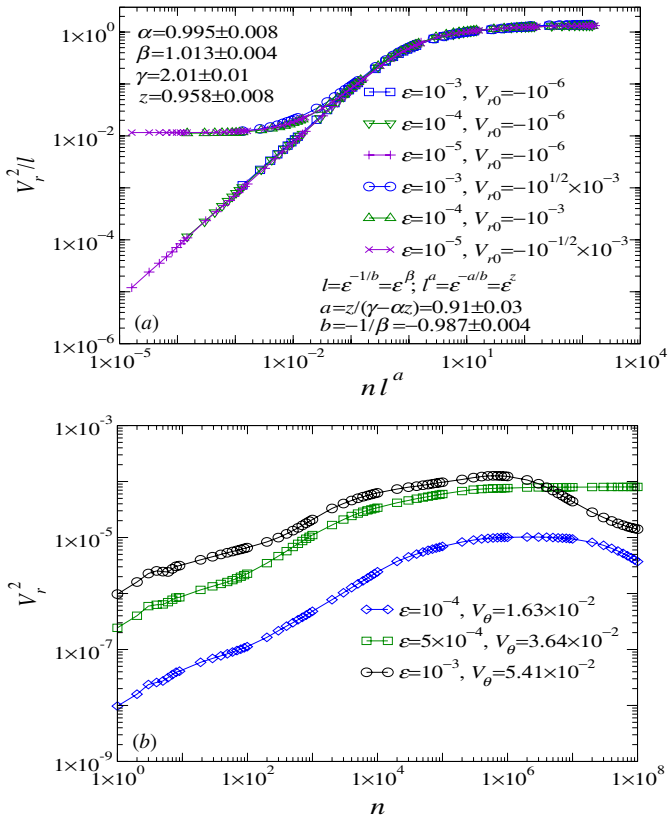

Figure 6. (*a*) Collapse of the V_r^2 displayed in figure 4(*b*) for $V_\theta < V_{\theta c}$. (*b*) V_r^2 curves for $V_\theta > V_{\theta c}$.

where $c = b/2$. Figure 6(*a*) shows the collapse of the V_r^2 curves originally displayed in figure 4(*b*) with $l = \varepsilon^{-1/b}$. Thus, for $V_\theta < V_{\theta c}$ we have the scaling exponents set

$$\begin{aligned} a &= z/(\gamma - \alpha z) = 0.91 \pm 0.03 \\ b &= -1/\beta = -0.987 \pm 0.004 \\ c &= b/2 = -0.494 \pm 0.002. \end{aligned} \tag{29}$$

The limit situation $V_\theta = 0$ reduces the system to the one-dimensional Fermi–Ulam model. Thus for $V_\theta \to 0$, it is expected that the scaling description of SBCB is the same as that of the Fermi–Ulam model. On the other hand, the dimension of the system is, in general, relevant to determine the scaling exponents. Since for the simplified one-dimensional Fermi–Ulam model the scaling exponents are $a = 0.99 \pm 0.03$, $b = -0.977 \pm 0.006$ and $c = -0.489 \pm 0.003$ [21, 22], we observe, within the uncertainties, that both one- and two-dimensional versions of the Fermi–Ulam model are basically described by the same exponent set.

We also evaluated the average quantity V_r^2 for $V_\theta > V_{\theta c}$. Figure 6(*b*) displays the results for different values of ε and $V_\theta > V_{\theta c}$, as indicated in the legend. The chosen initial conditions that generated each curve in figure 6(*b*) belong to the chaotic sea of SBCB. In limit of big values of V_θ we observe numerically that there are regions in the chaotic sea where the trajectories remain for a large number of collisions. Such a behavior affects the average quantity V_r^2

originating the irregular curves that we observe in figure 6(*b*). Thus the values of saturation $V^2_{r\mathrm{sat}}$ and crossover n_x cannot be satisfactorily obtained, as well as the scaling exponents.

5. Summary

We studied some properties of the lowest energy chaotic sea of the SBCB. The system is described by two control parameters, V_θ and ε. The position of the FISC depends on both V_θ and ε. For each value of ε there is a $V_\theta = V_{\theta c}$ where the size of the lowest chaotic region changes abruptly. For $V_\theta < V_{\theta c}$ the position of the FISC does not depend on V_θ and for $V_\theta > V_{\theta c}$ the chaotic sea breaks into minor chaotic regions separated by spanning curves. For $V_\theta \gtrsim V_{\theta c}$ these chaotic regions are very close and even numerical errors eventually merge them. Moreover we cannot use arbitrary large values of V_θ in the SBCB because the particle has only a small displacement in the circle even for a very large number of collisions.

By using a first-order expansion in the Taylor series, near the FISC with $V_\theta < V_{\theta c}$ and $V_\theta > V_{\theta c}$, we showed that appropriate variable transformations locally turn the SBCB map into the standard map.

We employed scaling analysis to describe the average properties of the SBCB low energy chaotic sea. The exponents describing the scaling of SBCB for $V_\theta < V_{\theta c}$ are essentially the same as those of the one-dimensional version of the Fermi–Ulam model [21, 22]. This is an unexpected result, if we consider that dimensionality is, in general, very important to determine scaling exponents. On the other hand, this result is consistent with the fact that the SBCB is equivalent to the Fermi–Ulam model when $V_\theta \to 0$. For large values of V_θ, we observe regions in the chaotic sea where orbits remain for a large number of collisions . Thus for $V_\theta > V_{\theta c}$, we were not able to obtain the scaling properties of the SBCB due to the irregular behavior of the V^2_r curves for large values of n.

Acknowledgments

D G L thanks Conselho Nacional de Desenvolvimento Científico, CNPq, for financial support. J K L da Silva thanks Fundação de Amparo à Pesquisa do Estado de Minas Gerais (FAPEMIG) and CNPq, Brazilian agencies, for partial financial support.

References

[1] Fermi E 1949 *Phys. Rev.* **75** 1169
[2] Lichtenberg A J and Lieberman M A 1992 *Regular and Chaotic Dynamics* (*Appl. Math. Sci.* vol 38) (New York: Springer)
[3] Lieberman M A and Lichtenberg A J 1972 *Phys. Rev.* A **5** 1852
[4] Pustylnikov L D 1978 *Trans. Moscow Math. Soc.* **2** 1
[5] Douady R 1982 Applications du théorème des tores invariants, Thèse de 3ème Cycle, Univ. Paris VII
[6] Saif F 2005 *Phys. Rep.* **419** 207
Saif F 2006 *Phys. Rep.* **425** 369
[7] Lichtenberg A J, Lieberman M A and Cohen R H 1980 *Physica* D **1** 291
[8] Ladeira D G and da Silva J K L 2007 *J. Phys. A: Math. Theor.* **40** 11467
[9] Sinai Y G 1970 *Russ. Math. Surveys* **25** 137
[10] Prosen T and Robnik M 1994 *J. Phys. A: Math. Gen.* **27** 8059
[11] Koiller J, Markarian R, Kamphorst S O and de Carvalho S P 1996 *J. Stat. Phys.* **83** 127
[12] Kamphorst S O and de Carvalho S P 1999 *Nonlinearity* **12** 1363
[13] Loskutov A, Ryabov A B and Akinshin L G 1999 *J. Exp. Theor. Phys.* **89** 966
[14] Loskutov A, Ryabov A B and Akinshin L G 2000 *J. Phys. A: Math. Gen.* **33** 7973
[15] de Carvalho R E, de Souza F C and Leonel E D 2006 *J. Phys. A: Math. Gen.* **39** 3561

[16] de Carvalho R E, de Souza F C and Leonel E D 2006 *Phys. Rev.* E **73** 066229
[17] Lenz F, Diakonos F K and Schmelcher P 2008 *Phys. Rev. Lett.* **100** 014103
[18] Kamphorst S O, Leonel E D and da Silva J K L 2007 *J. Phys. A: Math. Theor.* **40** F887–93
[19] Leonel E D, da Silva J K L and Kamphorst S O 2004 *Physica* A **331** 435
[20] Chirikov B V 1979 *Phys. Rep.* **52** 263
[21] Leonel E D, McClintock P V E and da Silva J K L 2004 *Phys. Rev. Lett.* **93** 14101
[22] da Silva J K L, Ladeira D G, Leonel E D, McClintock P V E and Kamphorst S O 2006 *Braz. J. Phys.* **36** 700
[23] Ladeira D G and da Silva J K L 2006 *Phys. Rev.* E **73** 026201
[24] Leonel E D and da Silva J K L 2003 *Physica* A **323** 181
[25] Leonel E D and McClintock P V E 2004 *Phys. Rev.* E **70** 016214
[26] Leonel E D 2007 *Phys. Rev. Lett.* **98** 114102